

A priori bond-valence and bond-length calculations in rock-forming minerals

Olivier Charles Gagné,^{a,*‡} Patrick H. J. Mercier^b and Frank Christopher Hawthorne^a

^aGeological Sciences, University of Manitoba, 125 Dysart Road, Winnipeg, Manitoba R3T 2N2, Canada, and ^bNational Research Council Canada, 1200 Montreal Road, Ottawa, Ontario K1A 0R6, Canada. *Correspondence e-mail: ogagne@carnegiescience.edu

Received 8 June 2018

Accepted 18 July 2018

Edited by A. J. Blake, University of Nottingham, England

‡ Current address: Geophysical Laboratory, Carnegie Institution for Science, 5251 Broad Branch Road NW, Washington, DC 20015, USA.

Keywords: bond valence; bond length; network equations; Lewis acidity; structural strain.

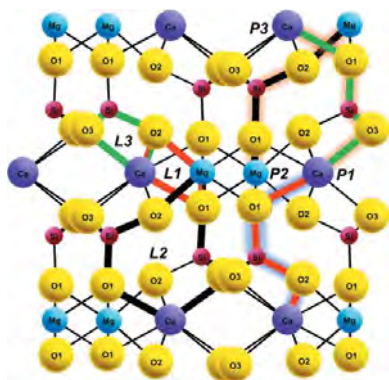
Supporting information: this article has supporting information at journals.iucr.org/b

Within the framework of the bond-valence model, one may write equations describing the valence-sum rule and the loop rule in terms of the constituent bond valences. These are collectively called the *network equations*, and can be solved for a specific bond topology to calculate its *a priori* bond valences. *A priori* bond valences are the ideal values of bond strengths intrinsic to a given bond topology that depend strictly on the formal valences of the ion at each site in the structure, and the bond-topological characteristics of the structure (*i.e.* the ion connectivity). The *a priori* bond valences are calculated for selected rock-forming minerals, beginning with a simple example (magnesiocromite, = 1.379 bits per atom) and progressing through a series of gradually more complex minerals (grossular, diopside, forsterite, fluoro-phlogopite, phlogopite, fluoro-tremolite, tremolite, albite) to finish with epidote (= 4.187 bits per atom). The effects of weak bonds (hydrogen bonds, long Na⁺–O²⁻ bonds) on the calculation of *a priori* bond valences and bond lengths are examined. For the selected set of minerals, *a priori* and observed bond valences and bond lengths scatter closely about the 1:1 line with an average deviation of 0.04 v.u. and 0.048 Å and maximum deviations of 0.16 v.u. and 0.620 Å. The scatter of the corresponding *a priori* and observed bond lengths is strongly a function of the Lewis acidity of the constituent cation. For cations of high Lewis acidity, the range of differences between the *a priori* and observed bond lengths is small, whereas for cations of low Lewis acidity, the range of differences between the *a priori* and observed bond lengths is large. These calculations allow assessment of the strain in a crystal structure and provide a way to examine the effect of bond topology on variation in observed bond lengths for the same ion-pair in different bond topologies.

1. Introduction

The bond-valence model (Brown, 2002, 2016) is used extensively in crystallography and mineralogy to validate structural arrangements in crystals, and to interpret many aspects of crystal structure in terms of constituent chemical composition and bond topology. There are two distinct aspects of the bond-valence model: (1) relating observed bond lengths to bond valences through experimentally determined bond-valence curves (*e.g.* Brown & Shannon, 1973; Brown & Altermatt, 1985; Brese & O'Keeffe, 1991; Gagné & Hawthorne, 2015), and (2) using bond-valence theory to understand chemical and topological aspects of atomic arrangements.

There are two important theorems in the bond-valence model (Brown, 2002, 2016): [1] the valence-sum rule, which states that *the sum of the bond valences at each atom is equal to the magnitude of the atomic valence*, and [2] the loop rule which states *the*



© 2018 International Union of Crystallography

sum of the directed bond valences around any circuit (closed path) of bonds in a structure is zero. One may write equations describing the valence-sum rule and the loop rule in terms of the constituent bond valences. These are collectively called the *network equations*, and can be solved to calculate *a priori* bond valences for a crystal structure. *A priori* bond valences are the ideal values of bond strengths intrinsic to a given crystal structure, and depend strictly on the formal valences of the ion at each site in the structure, and the bond-topological characteristics of the structure (*i.e.* the ion connectivity). From knowledge of the *a priori* bond valences of a crystal structure, one may use the bond-length–bond-valence correlation of the bond-valence model (above) to calculate the *a priori* bond lengths of the crystal structure. This approach has not been used very extensively; where it has been used, it has been applied to relatively simple structures, *e.g.* $(\text{H}_5\text{O}_2)_2\text{SO}_4$, $\text{CaMgSi}_2\text{O}_6$, $\text{K}_2\text{S}_5\text{O}_{16}$, $\text{Na}_2\text{B}_4\text{O}_7$, $\text{Na}_2\text{PO}_3\text{F}$, CaCrF_5 and TeI_4 (Brown, 1977), KVO_3 (Rutherford, 1990), $\text{Ca}_2\text{B}_2\text{Si}_2\text{O}_8$, $\text{Sr}_3\text{Ti}_2\text{O}_7$, $\text{Ba}_2\text{FeSi}_2\text{O}_7$, $\text{Sr}_3\text{Zr}_2\text{O}_7$, $\text{Y}_2\text{SiBe}_2\text{O}_7$ and KFeFPO_4 (Urusov & Orlov, 1999), tourmaline (Bosi & Lucchesi, 2007), scapolite (Hawthorne & Sokolova, 2008), milarite (Gagné & Hawthorne, 2016a). Here, we use *a priori* bond-valence calculations to calculate *a priori* bond lengths in a series of rock-forming minerals of different complexity [as measured by the topological information content; Krivovichev (2012, 2013)] and degrees of complication.

Our motivation for making these calculations is not to try and accurately predict observed bond valences. *A priori* bond valences are calculated from the network equations that describe the valences of ions at the sites in the structure and the connectivity of the chemical bonds involving those ions. As a result, the *a priori* bond valences are the ideal bond valences arising from the topology of the structure. However, the structure also has to conform to the symmetry of its space group, and embedding the topological structure into a space group causes strain (Brown, 2002, 2016). That strain is the difference between the *a priori* bond valences and the observed bond valences, and to calculate this strain it is necessary to derive the *a priori* bond valences. Here, we provide a readily accessible method to do this on the large scale that is necessary to quantitatively understand the general relation between structure topology, space-group symmetry and strain.

Bond-valence parameters used in this work are taken from Gagné & Hawthorne (2015) and Lewis acidities are taken from Gagné & Hawthorne (2017b).

2. Predicting bond length *via* bond-strength methods

The prediction of bond lengths has long fascinated mineralogists and crystallographers. Today, bond lengths are routinely predicted and rationalized *via* the addition of the constituent ionic radii (Shannon, 1976) based on the assumption that these values are transferable between crystal structures [see Gagné & Hawthorne 2017(a) for a discussion of the effect of structure type on mean bond length]. More sophisticated predictions of (individual) bond lengths take

into account local coordination (*e.g.* Baur, 1970, 1971, 1981; Brown & Shannon, 1973), and are typically rooted in the consideration of a crystal structure as a topological *network* where nodes and edges are represented by atoms and bonds, respectively. Mackay & Finney (1973) proposed modelling crystal structures as networks subject to Kirchhoff's circuit laws, and solved Kirchhoff's voltage and current equations to obtain the fluxes (bond strengths) for BaTiO_3 . This approach was reformulated within the framework of the bond-valence model by Brown (1977), who realized that Kirchhoff's voltage law does not apply to chemical networks. Brown proposed the 'equal-valence rule' as an alternative, where the bond valences incident at an ion tend to be *as nearly equal as possible*. A justification based on the equal capacitance of bonds based on the principle of maximum symmetry is given by Brown (2016). Although the equations derived from Kirchhoff's voltage law and Brown's equal-valence rule are in practice identical, the equal-valence rule is at an advantage of being more physically grounded.

Brown (1977) proposed an iterative approach in solving for the *a priori* bond valences of a crystal structure, which consists of averaging the cation and anion Pauling bond strength of individual bonds, and changing these values by small increments (in cycles) until the valence-sum rule is obeyed for all cation and anions of the structure. O'Keeffe (1990) and Rutherford (1990) proposed a more direct approach to the solution of the network equations that essentially consists of solving a system of equations *via* matrix manipulations. To deal with negative bond valences sometimes encountered in structures with very weak bonds (*e.g.* a negative value for the K–O1 bond in KVO_3), Rutherford introduced weighting factors for the bond valences of the loop equations to have the *a priori* bond valences more closely match the observed bond valences; this is equivalent to allowing non-integer values in the connectivity matrix for the loop equations). However, this practice is unreliable as it allows one to obtain any desired solution for the *a priori* bond valences; although the valence-sum equations remain satisfied, one (or more) loop equation deviates significantly from 0, by an arbitrary amount. O'Keeffe (1990) used a different weighting scheme whereby the bond valences of the loop equations are weighted according to their Pauling bond strength. Although using such weighting produces closer agreement with observed bond valences, one cannot then use the difference between the resulting *a priori* and observed bond valences as a measure of structural strain. For this reason, we use the method of Brown (1977), in which the loop equations are constrained to be equal to 0 and the bond valences are unweighted.

The methods of O'Keeffe (1990) and Rutherford (1990) may be reformulated without the introduction of weighting factors (discussed further below). Urusov & Orlov (1999) used this approach to solve for the *a priori* bond valences of $\text{Ca}_2\text{B}_2\text{Si}_2\text{O}_8$ and to calculate its *a priori* bond lengths. The same method was used by Gagné and Hawthorne (2016a) to solve for the *a priori* bond lengths of 14 milarite-group minerals. Methods alternative to the use of loop equations include the resonance-bond model (Rutherford, 1998) and the method of

Table 1
Bond valences for magnesiochromite.

	Mg	Cr	Σ an
O1	$a^{\times 4\downarrow}$	$b^{\times 6\downarrow \times 3 \rightarrow}$	2
Σ cat	2	3	

Table 2
A priori and observed bond valences for magnesiochromite.

Site	<i>A priori</i> bond valence (v.u.)	<i>A priori</i> bond length (Å)	Observed bond valence (v.u.)	Observed bond length (Å) [†]
Mg <i>a</i>	0.5	1.915	0.445	1.967
Cr <i>b</i>	0.5	1.904	0.475	1.994

[†] Bond lengths from Nestola *et al.* (2014).

maximum entropy (Rao & Brown, 1998), but these have seen little use.

3. Solution of the network equations

There are two cases arising in solving the network equations of a crystal structure: (1) valence-sum equations are sufficient for solution (*i.e.* loop equations are redundant linear combinations of valence-sum equations), and (2) a combination of valence-sum and loop equations is necessary for solution. We discuss the two cases below.

3.1. Calculation of *a priori* bond valences from valence-sum equations

The valence-sum rule states that *the sum of the bond valences at each atom is equal to the magnitude of the atomic valence*. One may write a set of equations describing the valence-sum rule in terms of the constituent bond valences. This gives a system of equations involving the bond valences, and one may calculate bond valences from these network equations; these are known as *a priori* bond valences.

The n equations of the valence-sum rule may be written in general form as follows:

$$\sum_j s_{ij} = V_i \quad (i = 1 \text{ to } n), \quad (1)$$

where the summation involves all bonds from the central ion i to the coordinating ions j for the n crystallographically distinct ions in the structure. We will now look at various sets of equations and their solution for minerals of increasing complexity.

3.1.1. Magnesiochromite. Magnesiochromite, ideally $\text{MgCr}^{3+}_2\text{O}_4$, is cubic, space group $Fd\bar{3}m$, has the normal spinel structure, = 1.379 bits per atom (Krivovichev, 2013); Mg is tetrahedrally coordinated and has only one symmetrically distinct Mg–O bond; Cr^{3+} is octahedrally coordinated and has one symmetrically distinct Cr^{3+} –O bond. The bond-valence table is shown in Table 1. The bond valences are represented by the variables a and b . The formal charges of the cations at the cation sites are written as $^{\text{site}}V$: $^{\text{Mg}}V$ and $^{\text{Cr}}V$ and the charges of the anions are constrained to be equal to their formal valences. As there is only one symmetrically distinct

Table 3
Bond-valence table for grossular.

	Ca	Al	Si	Σ an
O	$a^{\times 8\downarrow \times 2 \rightarrow}$	$b^{\times 6\downarrow}$	$c^{\times 4\downarrow}$	2
Σ cat	2	3	4	

Table 4
A priori and observed bond valences for grossular.

Site	<i>A priori</i> bond valence (v.u.)	<i>A priori</i> bond length (Å)	Observed bond valence (v.u.)	Observed bond length (Å) [†]
Ca <i>a</i>	0.25	2.474	0.365, 0.239	2.319, 2.493
Al <i>b</i>	0.5	1.905	0.479	1.921
Si <i>c</i>	1	1.624	0.942	1.647

[†] Bond lengths from Meagher (1975).

bond for each of the Mg and Cr^{3+} coordination polyhedra, there are three valence-sum equations:

$$4a = ^{\text{Mg}}V = 2 \quad [v1]$$

$$6b = ^{\text{Cr}}V = 3 \quad [v2]$$

$$a + 3b = 2 \quad [v3]$$

One of the valence-sum equations is linearly dependent of the others because of the constraint of electroneutrality. Hence there are two unknowns and two independent equations. The *a priori* bond valences are as follows: Mg–O : $^{\text{Mg}}V/4 = 2/4 = 0.5$ v.u.; $\text{Cr}^{3+}\text{–O}$: $^{\text{Cr}}V/6 = 3/6 = 0.5$ v.u.; $a + 3b = 2 = ^{\text{O}}V$. The resulting *a priori* bond lengths (using the bond-valence parameters of Gagné & Hawthorne, 2015) are shown in Table 2 together with the observed bond lengths and bond valences calculated from the structure of Nestola *et al.* (2014).

3.1.2. Grossular. Grossular, ideally $\text{Ca}_3\text{Al}_2\text{Si}_3\text{O}_{12}$, cubic, space group $Ia\bar{3}d$, $I_G = 1.595$ bits per atom; Ca is [8]-coordinated with two crystallographically distinct Ca–O distances, Al is [6]-coordinated with one crystallographically distinct Al–O distance, and Si is [4]-coordinated with one crystallographically distinct Si–O distance. There are four distinct cation–oxygen distances, but the two distinct Ca–O distances are topologically identical, and hence we must treat Ca as having eight topologically identical bonds. In the resulting bond-valence table (Table 3), there are four valence-sum equations:

$$8a = ^{\text{Ca}}V = 2 \quad [v1]$$

$$6b = ^{\text{Al}}V = 3 \quad [v2]$$

$$4c = ^{\text{Si}}V = 4 \quad [v3]$$

$$2a + b + c = 2 \quad [v4]$$

Again, one of the valence-sum equations is constrained to be linearly dependent of the others because of the constraint of electroneutrality. There are three unknowns and three

linearly independent equations, which again is sufficient to calculate the *a priori* bond valences from the valence-sum equations: Ca—O: ${}^{\text{Ca}}V/8 = 2/8 = 0.25$ v.u.; Al—O: ${}^{\text{Al}}V/6 = 3/6 = 0.5$ v.u.; ${}^{\text{Si}}V/4 = 4/4 = 1$ v.u.; $2a + b + c = 2 = {}^{\text{O}}V$. The resulting *a priori* bond lengths are shown in Table 4 together with the observed bond lengths and bond valences calculated from the structure of Meagher (1975).

3.2. Calculation of *a priori* bond valences from the valence-sum equations and the loop equations

3.2.1. Diopside. Diopside, ideally $\text{CaMgSi}_2\text{O}_6$, monoclinic, space group $C2/c$, = 2.522 bits per atom; Ca is [8]-coordinated with four crystallographically distinct Ca—O distances, Mg is [6]-coordinated with three crystallographically distinct Mg—O distances, and Si is [4]-coordinated with four crystallographically distinct Si—O distances. However, there are two pairs of Ca—O bonds (to O3) that are crystallographically distinct but topologically identical and hence there are only three Ca—O bond valences (*a*, *b* and *c*) in the bond-valence table (Table 5). There are two pairs of Mg—O bonds (to O1) and two Si—O bonds (to O3) that are similarly merged in the bond-valence table which thus has eight bond valences *a* through *h*.

The valence-sum rule for the cations gives us the following equations:

$$2a + 2b + 4c = {}^{\text{Ca}}V = 2 \quad [v1]$$

$$4d + 2e = {}^{\text{Mg}}V = 2 \quad [v2]$$

$$f + g + 2h = {}^{\text{Si}}V = 4 \quad [v3]$$

The valence-sum rule for the anions gives us the following equations:

$$a + 2d + f = 2 \quad [v4]$$

$$b + e + g = 2 \quad [v5]$$

$$2c + 2h = 2 \quad [v6]$$

These six equations are constrained by charge balance, and hence there are five linearly independent valence-sum equations, and the system is underdetermined. As a result, we must make use of the loop rule, which states *the sum of the directed bond valences around any circuit (closed path) of bonds in a structure is zero*. The equations for the loop rule may be written in general form as follows:

$$\sum s_{ij} = 0, \quad (2)$$

where the summation is over the directed bond valences around any circuit in the directed graph of the bond network of the structure. This rule introduces the idea of *directed bond valences*, whereby bonds from a cation to an anion are considered positive and bonds from an anion to a cation are considered negative in sign. The number of linearly independent loop equations is equal to the difference between the

Table 5
Bond valences for diopside.

	Ca	Mg	Si	Σ_{an}
O1	$a^{\times 2\downarrow}$	$d^{\times 4\downarrow \times 2\rightarrow}$	f	2
O2	$b^{\times 2\downarrow}$	$e^{\times 2\downarrow}$	g	2
O3	$c^{\times 4\downarrow \times 2\rightarrow}$		$h^{\times 2\downarrow \times 2\rightarrow}$	2
Σ_{cat}	2	2	4	

number of crystallographically distinct bonds and sites in the crystal (Rutherford, 1990). Thus to solve for the *a priori* bond valences of diopside, we need three linearly independent loop equations of the form of equation (2). Consider the structure of diopside shown in Fig. 1. Three loops are shown by the heavy coloured lines in this figure and indicated by the symbols L1–L3. The loop equations are as follows:

Loop 1 (red): Ca → O1 → Mg → O2 → Ca, resulting in the following loop equation:

$$a - d + e - b = 0 \quad [L1]$$

Loop 2 (black): Ca → O1 → Si → O2 → Mg → O1 → Si → O3 → Ca, resulting in the following loop equation:

$$a - f + g - e + d - f + h - c = 0 \quad [L2]$$

Loop 3 (green): Ca → O2 → Si → O3 → Ca, resulting in the following loop equation:

$$b - g + h - c = 0 \quad [L3]$$

Thus we have eight equations and eight unknowns, and we may solve these equations for the *a priori* bond valences.

3.2.2. Solution of the network equations for diopside. For large systems of equations, it becomes efficient to represent

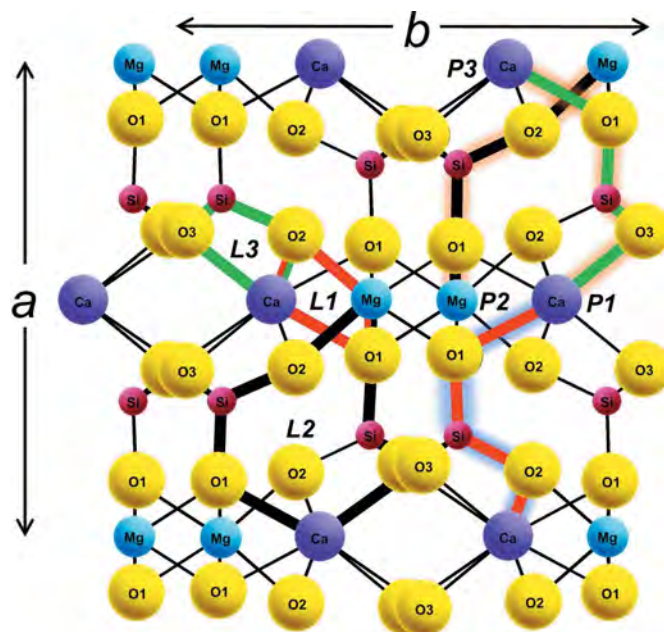


Figure 1
The crystal structure of diopside showing the loops L1, L2 and L3 as heavy coloured lines and the paths P1, P2 and P3 as heavy coloured lines outlined by a nimbus of contrasting colour.

Table 6
A priori and observed bond valences for diopside.

Site		<i>A priori</i> bond valence (v.u.)	<i>A priori</i> bond length (Å)	Observed bond valence (v.u.)	Observed bond length (Å) [†]
Ca	<i>a</i>	0.325	2.367	0.330	2.360
	<i>b</i>	0.425	2.257	0.337	2.352
	<i>c</i>	0.125	2.758	0.202, 0.138	2.561, 2.717
Mg	<i>d</i>	0.300	2.141	0.357, 0.318	2.064, 2.115
	<i>e</i>	0.400	2.014	0.369	2.050
	<i>f</i>	1.075	1.596	1.058	1.602
Si	<i>g</i>	1.175	1.561	1.108	1.584
	<i>h</i>	0.875	1.676	0.902, 0.850	1.664, 1.687

[†] Bond lengths from Clark *et al.* (1969).

the network equations in matrix form $\mathbf{Ax} = \mathbf{b}$, where the \mathbf{A} matrix contains the coefficients of the network equations, the left-side column vector \mathbf{x} contains the *a priori* bond valences (unknown) and the right-side column vector \mathbf{b} contains the formal charges of the ions at the sites, together with the zeros associated with the loop equations. For diopside, this gives

$$\begin{bmatrix} 2 & 2 & 4 & 0 & 0 & 0 & 0 & 0 \\ 0 & 0 & 0 & 4 & 2 & 0 & 0 & 0 \\ 0 & 0 & 0 & 0 & 0 & 1 & 1 & 2 \\ 1 & 0 & 0 & 2 & 0 & 1 & 0 & 0 \\ 0 & 1 & 0 & 0 & 1 & 0 & 1 & 0 \\ 1 & -1 & 0 & -1 & 1 & 0 & 0 & 0 \\ 1 & 0 & -1 & 1 & -1 & -2 & 1 & 1 \\ 0 & 1 & -1 & 0 & 0 & 0 & -1 & 1 \end{bmatrix} \begin{bmatrix} a \\ b \\ c \\ d \\ e \\ f \\ g \\ h \end{bmatrix} = \begin{bmatrix} 2 \\ 2 \\ 4 \\ 2 \\ 2 \\ 0 \\ 0 \\ 0 \end{bmatrix} \quad (3)$$

where rows 1–3 and 4–5 of the \mathbf{A} matrix are for the valence-sum equations of the cations ([v1]–[v3]) and anions ([v4]–[v5]), respectively, and rows 6–8 are for the loop equations ([L1]–[L3]), with a sum of 0 in the column matrix \mathbf{b} . We arbitrarily omitted valence-sum equation [v6] based on redundancy caused by the constraint of electroneutrality; however, any one of the six valence-sum equations could have been omitted (we list equations in the \mathbf{A} matrix in the above order from hereon). From here, we solve for \mathbf{x} via the following manipulation: $\mathbf{A}^{-1}\mathbf{Ax} = \mathbf{A}^{-1}\mathbf{b} = \mathbf{x}$. Table 6 shows the results of this calculation, together with the *a priori* bond lengths calculated using the bond-valence parameters of Gagné & Hawthorne (2015), and the observed bond lengths and bond valences calculated from the structure of Clark *et al.* (1969).

3.2.3. Generalization of the loop rule. As noted above, the loop rule involves the summation of directed bond valences around any circuit in the digraph of the bond network of the structure. As noted by Mackay & Finney (1973), this is the structural analogue of Kirchoff's second rule. However, an electrical network is not an exact analogue of the network of chemical bonds and ions in a crystal structure; in the latter, many vertices (corresponding to ions) are symmetrically equivalent. This in turn would indicate that the loop rule, *i.e.* summation of directed bond valences around any circuit in the digraph is zero, is just a special case of the more general rule that the summation of directed bond valences around any path with symmetrically equivalent terminal vertices is zero. We

tested this idea and found that we get the same solution for the *a priori* bond valences irrespective of whether we use loops or paths with symmetrically equivalent terminal vertices. Thus we may replace the loop equations [L1]–[L3] above by the following path equations [P1]–[P3] (where each path has symmetrically equivalent terminal vertices):

Path 1 (red): Ca → O1 → Si → O2 → Ca, resulting in the following equation:

$$a - f + g - b = 0 \quad [P1]$$

Path 2 (black): Mg → O1 → Si → O2 → Mg, resulting in the following equation:

$$d - f + g - e = 0 \quad [P2]$$

Path 3 (green): Ca → O(1) → Si → O(3) → Ca, resulting in the following equation:

$$a - f + h - c = 0 \quad [P3]$$

The paths are shown on Fig. 1 by the heavy coloured lines outlined by a nimbus of contrasting colour and indicated by the symbols P1–P3 adjacent to the starting ions for each path. Replacing loop equations [L1]–[L3] in equation (3) by path equations [P1]–[P3] gives the same solution for the *a priori* bond valences. Thus we may generalize the loop rule of the bond-valence model as follows: *the sum of the directed bond valences along any path of bonds in a structure is zero where the path begins and ends on symmetrically equivalent terminal ions.* Moreover, the term 'loop equations' are not sufficiently general to encompass both loops and paths with symmetrically equivalent terminal ions; we suggest replacing the word loop by path, *i.e.* path equations; a loop is subsumed in this definition, as a loop is a path that begins and ends on the same terminal ion.

3.2.4. Derivation of the linearly independent paths with symmetrically equivalent terminal ions. Brown (2002) described the derivation of linearly independent path equations via a spanning tree method, for CaCrF₅. However, we find this method becomes impractical for complicated structures. Alternatively, visually navigating crystal structures for loops and paths is time-consuming. Below, we describe a working method that allows the derivation of all linearly independent (and no linearly dependent) path equations of a crystal structure from its bond topology table in a matter of seconds (for a trained user), for crystal structures of any level of complexity.

The general idea is the following: derive cycles in the bond topology table by navigating through the variables (disregarding multiplicity), alternating vertical (+) and horizontal (–) moves and producing the shortest cycles possible (length 4, 6, 8, [...]). The sampling order of starting points is from left to right, up to down, and the first two moves must be right and down (by convention); the other moves are arbitrary and depend on the minimum path length achievable. One may not go to variables above the starting row, and the path is to be closed by going up to the starting variable. Thus the left-most variable of row 1 is the first starting point, from which a path equation is derived, if possible; upon failure, *e.g.* for the right-

most variable of any given row, one moves to the next starting point. This is to be repeated using all variables as starting points.

The above method follows a certain set of arbitrary rules, some of which arise from dealing with a system of equations that follows the rules of permutability (for rows and columns). It is possible to derive a different but similar set of path equations by either permuting rows and columns, or using slight modifications of the above method. However, all sets of equations will have the same solution for the *a priori* bond valences.

Alternatively, one may derive all possible cycles of length 4, 6, 8, [...] in the bond topology table, followed by reducing all gathered equations to linearly independent ones *via* standard methods.

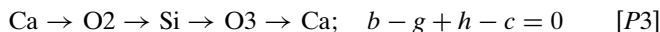
We may now go back to diopside, and use these rules to derive three path equations from the bond topology table. We start at the first row and first column of the bond-valence table (Table 5):



Next we move to the first row second column:



There is no linearly independent equation possible starting from the last column of the first row, and we move on to the second row, first column:



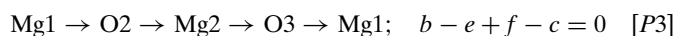
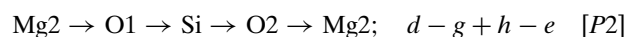
This brings the total to three equations, and a quick check shows that no other starting points in rows 2 and 3 can yield new equations according to the given set of rules. The *a priori* bond valences that result from using these three path equations are the same as those using the three path equations derived visually (above), as well as those using loop equations [L1]–[L3].

3.2.5. Forsterite. Forsterite, ideally Mg_2SiO_4 , orthorhombic, space group $Pbnm$, = 2.522 bits per atom; there are two Mg sites, both of which are [6]-coordinated and one tetrahedrally coordinated Si site. The topologies of the magnesiochromite (spinel) and forsterite (olivine) structures are the same. However, when dealing with the olivine structure, it is necessary to keep the topologically equivalent octahedrally coordinated sites $M1$ and $M2$ different. This is not important for forsterite–fayalite $(\text{Mg}, \text{Fe}^{2+})_2\text{SiO}_4$ where the octahedrally coordinated cations are disordered, but it is important for olivine minerals such as monticellite (CaMgSiO_4) and kirschsteinite $\text{CaFe}^{2+}\text{SiO}_4$ in which Mg and Fe^{2+} occur at $M1$ and Ca occurs at $M2$. The resulting strain issues would be lost without retention of $M1$ and $M2$ as separate sites. This issue does not arise where topologically identical sites are occupied by O^{2-} where the sites may be merged in the bond-valence table. Mg2 has two symmetrically distinct pairs of bonds to O3, but these bonds are topologically identical and hence they are merged in the bond-valence table. The bond-valence table (Table 7) has nine independent bond valences a through i , there are six valence-sum equations, but one is linearly

Table 7
Bond valence for forsterite.

	Mg1	Mg2	Si	Σ an
O1	$a^{\times 2\downarrow \times 2 \rightarrow}$	d	g	2
O2	$b^{\times 2\downarrow \times 2 \rightarrow}$	e	h	2
O3	$c^{\times 2\downarrow}$	$f^{\times 4\downarrow \times 2 \rightarrow}$	$i^{\times 2}$	2
Σ cat	2	2	4	

dependent of the others. There are nine unknowns and five independent equations, and hence the system needs four additional path equations. Using the above rules, these paths may be derived:



Omitting the O3 valence-sum equation as redundant, we have:

$$\begin{bmatrix} 2 & 2 & 2 & 0 & 0 & 0 & 0 & 0 & 0 \\ 0 & 0 & 0 & 1 & 1 & 4 & 0 & 0 & 0 \\ 0 & 0 & 0 & 0 & 0 & 0 & 1 & 1 & 2 \\ 2 & 0 & 0 & 1 & 0 & 0 & 1 & 0 & 0 \\ 0 & 2 & 0 & 0 & 1 & 0 & 0 & 1 & 0 \\ 1 & -1 & 0 & -1 & 1 & 0 & 0 & 0 & 0 \\ 0 & 0 & 0 & 1 & -1 & 0 & -1 & 1 & 0 \\ 0 & 1 & -1 & 0 & -1 & 1 & 0 & 0 & 0 \\ 0 & 0 & 0 & 0 & 1 & -1 & 0 & -1 & 1 \end{bmatrix} \begin{bmatrix} a \\ b \\ c \\ d \\ e \\ f \\ g \\ h \\ i \end{bmatrix} = \begin{bmatrix} 2 \\ 2 \\ 4 \\ 2 \\ 2 \\ 0 \\ 0 \\ 0 \\ 0 \end{bmatrix}, \quad (4)$$

where rows 1–3 and 4–5 of the \mathbf{A} matrix are for the valence-sum equations of the cations and anions, respectively, and rows 6–9 are for the path equations [P1]–[P4]. Table 8 shows the solution to these equations, together with the *a priori* bond lengths calculated using the bond-valence parameters of Gagné & Hawthorne (2015), and the observed bond lengths and the bond valences calculated from the structure of Smyth & Hazen (1973).

3.2.6. Fluoro-phlogopite. Ideally $\text{KMg}_3\text{AlSi}_3\text{O}_{10}\text{F}_2$, simplest polytype monoclinic 1M, space group $C2/m$, = 2.822 bits per atom for fluoro-phlogopite; there is one K site that is [12]-coordinated, two Mg sites that are [6]-coordinated by four O^{2-} and two F^- anions, one T site that is [4]-coordinated and occupied by Si^{4+} and Al^{3+} . There is one site that may be occupied by F^- which is coordinated by three Mg^{2+} ions. K^+ has two sets of symmetrically equivalent bonds to O1, each with a multiplicity of 4; however, these two sets of bonds are topologically identical. Similarly, K has two sets of symmetrically equivalent bonds to O3, each with a multiplicity of 2; these two sets of bonds are also topologically identical. Topologically identical bonds are merged in the bond-valence table (Table 9) used for the *a priori* bond-valence calculation. Mg2 has two sets of symmetrically equivalent bonds to O3,

Table 8
A priori and observed bond valences for forsterite.

Site		<i>A priori</i> bond valence (v.u.)	<i>A priori</i> bond length (Å)	Observed bond valence (v.u.)	Observed bond length (Å)†
Mg1	<i>a</i>	0.333	2.095	0.341	2.084
	<i>b</i>	0.333	2.095	0.354	2.068
	<i>c</i>	0.333	2.095	0.306	2.132
Mg2	<i>d</i>	0.333	2.095	0.274	2.182
	<i>e</i>	0.333	2.095	0.368	2.051
	<i>f</i>	0.333	2.095	0.255, 0.355	2.214, 2.067
Si	<i>g</i>	1.000	1.624	1.023	1.615
	<i>h</i>	1.000	1.624	0.928	1.653
	<i>i</i>	1.000	1.624	0.972	1.635

† Bond lengths from Smyth & Hazen (1973).

Table 9
 Bond valences for fluoro-phlogopite.

	K	Mg1	Mg2	Si/Al	Σan
O1	$a^{×8↓×2→}$			$g^{×2↓×2→}$	2
O2	$b^{×4↓×2→}$			$h^{×2→}$	2
O3		$c^{×4↓}$	$e^{×4↓×2→}$	<i>i</i>	2
F		$d^{×2↓}$	$f^{×2↓×2→}$		1
Σcat	1	2	2	3.75	

each with a multiplicity of 2; however, these two sets of bonds are topologically identical and are merged in Table 9.

The bond-valence table for fluoro-phlogopite (Table 9) has nine independent bond valences *a* through *i* and there are eight bond-valence equations of the type (1) to (6), see above. One of the bond-valence equations is linearly dependent of the others because of the constraint of electroneutrality. Hence the system of bond-valence equations is under-determined and we must include two path equations. These equations may be derived from the bond-valence table (Table 9) as discussed above, resulting in the following network equations:

$$\begin{bmatrix} 8 & 4 & 0 & 0 & 0 & 0 & 0 & 0 & 0 \\ 0 & 0 & 4 & 2 & 0 & 0 & 0 & 0 & 0 \\ 0 & 0 & 0 & 0 & 4 & 2 & 0 & 0 & 0 \\ 0 & 0 & 0 & 0 & 0 & 0 & 2 & 1 & 1 \\ 2 & 0 & 0 & 0 & 0 & 0 & 2 & 0 & 0 \\ 0 & 2 & 0 & 0 & 0 & 0 & 0 & 2 & 0 \\ 0 & 0 & 1 & 0 & 2 & 0 & 0 & 0 & 1 \\ 1 & -1 & 0 & 0 & 0 & 0 & -1 & 1 & 0 \\ 0 & 0 & 1 & -1 & -1 & 1 & 0 & 0 & 0 \end{bmatrix} \begin{bmatrix} a \\ b \\ c \\ d \\ e \\ f \\ g \\ h \\ i \end{bmatrix} = \begin{bmatrix} 1 \\ 2 \\ 2 \\ 3.75 \\ 2 \\ 2 \\ 2 \\ 0 \\ 0 \end{bmatrix} \quad (5)$$

where rows 1–4 and 5–7 of the **A** matrix are for the valence-sum equations of the cations and anions, respectively, and rows 8–9 are for the path equations (the valence-sum equation for the F site is omitted). Note that the above equations apply to phlogopite if the (OH)[−] group is treated as a single ion and the hydrogen bonding is ignored.

Table 10 shows the solution to these equations, together with the *a priori* bond lengths, the observed bond lengths and

Table 10
A priori and observed bond valences for fluoro-phlogopite.

Site		<i>A priori</i> bond valence (v.u.)	<i>A priori</i> bond length (Å)	Observed bond valence (v.u.)	Observed bond length (Å)†
K	<i>a</i>	0.083	3.035	0.092, 0.045	2.996, 3.284
	<i>b</i>	0.083	3.035	0.092, 0.045	2.995, 3.283
Mg1	<i>c</i>	0.333	2.095	0.343	2.082
	<i>d</i>	0.333	2.095	0.388	2.027
Mg2	<i>e</i>	0.333	2.095	0.352, 0.344	2.071, 2.081
	<i>f</i>	0.333	2.095	0.380	2.037
Si/Al	<i>g</i>	0.917	1.660	0.933	1.651
	<i>h</i>	0.917	1.660	0.933	1.651
	<i>i</i>	1.000	1.626	0.928	1.653

 † Bond lengths from Gianfagna *et al.* (2007).

Table 11
 Bond valences for tremolite.

	Ca	Mg1	Mg2	Mg3	Si1	Si2	H	Σan
O1		$e^{×2↓}$	$h^{×2↓}$	$k^{×4↓}$	<i>m</i>			2
O2	$a^{×2↓}$	$f^{×2↓}$	$i^{×2↓}$			<i>q</i>		2
O3		$g^{×2↓×2→}$		$l^{×2↓}$			<i>u</i>	2
O4	$b^{×2↓}$		$j^{×2↓}$			<i>r</i>		2
O5	$c^{×2↓}$				<i>n</i>	<i>s</i>		2
O6	$d^{×2↓}$				<i>o</i>	<i>t</i>	$w^{×2↓}$	2
O7					$p^{×2→}$		<i>v</i>	2
Σcat	2	2	2	2	4	4	1	

the bond valences calculated from the structure of Gianfagna *et al.* (2007).

3.2.7. Tremolite, fluoro-tremolite. Ideally $\text{Ca}_2\text{Mg}_5\text{Si}_8\text{O}_{22}(\text{OH},\text{F})_2$, monoclinic, space group $C2/m$, = 3.699 bits per atom for tremolite and 3.773 bits per atom for fluoro-tremolite; there is one Ca site that is [8]-coordinated, three Mg sites that are [6]-coordinated, two Si sites that are [4]-coordinated, and one site containing OH, the donor O of which is coordinated by three Mg atoms. There are no topological degeneracies among the bonds in tremolite. The H⁺ ion forms an OH[−] group with O3, making a hydrogen bond with O7 and possibly a hydrogen bond with O6. We will examine the effect of hydrogen bonds on *a priori* bond-valence calculations by solving the system of equations both with and without the consideration of hydrogen bonds. Here, it is most efficient to show the bond topology table with the maximum number of hydrogen bonds and to derive all network equations (including paths that use the hydrogen bonds). For cases where these hydrogen bonds are not considered, the matrices are updated without the relevant variables and their resulting paths (not shown here).

The bond-valence table (Table 11) has 23 independent bond valences *a* through *w* (variable *w* is listed before variable *v* in the bond topology table to indicate that it is the longest and weakest, thus most questionable bond). There are 14 bond-valence equations, one of which is dependent because of electroneutrality. The system of bond-valence equations is under-determined and we must derive $23 - (14 - 1) = 10$ path equations to solve for the *a priori* bond valences. Following the method above, we get

Table 16

A priori and observed bond valences for epidote without and with hydrogen bonds.

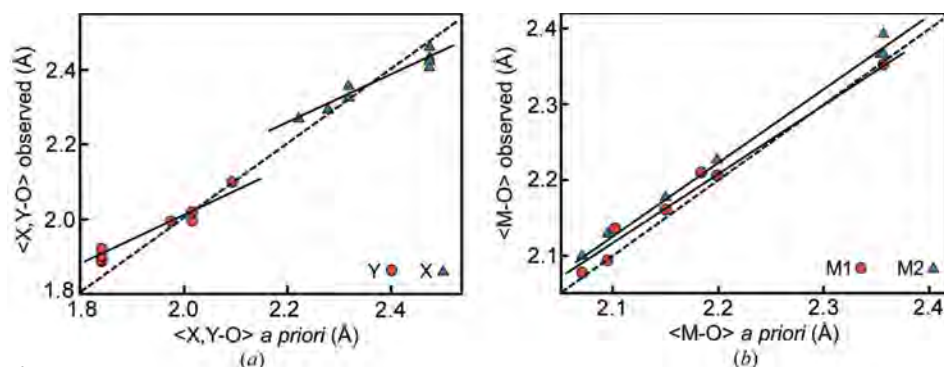
Site	<i>A priori</i> bond valence (v.u.)		<i>A priori</i> bond length (Å)		Observed bond valence (v.u.)	Observed bond length (Å)†	
	None	...O4	None	...O4			
Ca1	<i>a</i>	0.207	0.167	2.551	2.639	0.259	2.459
	<i>b</i>	0.252	0.299	2.472	2.401	0.357	2.329
	<i>c</i>	0.207	0.156	2.552	2.667	0.207	2.552
	<i>d</i>	0.155	0.213	2.670	2.540	0.098	2.856
	<i>e</i>	0.444	0.455	2.239	2.229	0.387	2.295
	<i>f</i>	0.092	0.122	2.881	2.767	0.069	3.002
Ca2	<i>g</i>	0.214	0.184	2.538	2.600	0.219, 0.116	2.528, 2.788
	<i>h</i>	0.158	0.163	2.663	2.650	0.164	2.646
	<i>i</i>	0.350	0.318	2.337	2.375	0.437	2.246
	<i>j</i>	0.209	0.186	2.548	2.596	0.066	3.018
	<i>k</i>	0.062	0.250	3.042	2.474	0.218	2.530
	<i>l</i>	0.408	0.412	2.088	2.059	0.264	2.225
Fe ³⁺	<i>m</i>	0.509	0.565	2.009	1.943	0.508	1.986
	<i>n</i>	0.662	0.479	1.914	2.003	0.581	1.937
	<i>o</i>	0.504	0.567	2.012	1.941	0.727	1.855
	<i>p</i>	0.416	0.481	1.977	1.921	0.460	1.939
	<i>q</i>	0.669	0.548	1.791	1.870	0.587	1.844
	<i>r</i>	0.415	0.470	1.977	1.930	0.438	1.958
Al1	<i>s</i>	0.564	0.500	1.858	1.905	0.569	1.854
	<i>t</i>	0.467	0.413	1.931	1.979	0.473	1.926
	<i>u</i>	0.469	0.587	1.930	1.842	0.546	1.870
Si1	<i>v</i>	0.969	0.939	1.636	1.648	0.935	1.650
	<i>w</i>	1.206	1.227	1.551	1.544	1.148	1.570
	<i>x</i>	0.855	0.894	1.685	1.667	0.974	1.634
Si2	<i>y</i>	1.027	1.038	1.613	1.609	1.018	1.617
	<i>z</i>	1.078	1.062	1.594	1.601	1.091	1.590
	<i>aa</i>	0.868	0.862	1.679	1.682	0.974	1.634
Si3	<i>ab</i>	1.063	1.068	1.600	1.598	0.994	1.626
	<i>ac</i>	0.962	0.904	1.639	1.663	0.900	1.665
	<i>ad</i>	0.911	0.961	1.660	1.639	0.957	1.641
H	<i>ae</i>	1.000	0.576	0.918	1.153	0.870	0.977
	<i>af</i>	–	0.424	2.551	1.284	0.084	1.973

† Bond lengths from Gatta *et al.* (2010).

4. Discussion

4.1. Agreement between observed and *a priori* bond lengths

It is important to realize that the calculation of *a priori* bond valences and bond lengths is not a prediction. It is a calculation that allows quantitative assessment of the strain in a crystal structure, an important quantity that Gagné & Hawthorne (2017a) suggest is strongly related to the variation in mean bond length for ion pairs in crystal structures.


Figure 2

Comparison of mean *a priori* bond lengths with observed bond lengths for (a) selected garnet structures, and (b) selected olivine structures. Broken line is $x = y$.

Table 17

Strain indices (v.u.) for the minerals/coordinations considered in this work.

	Global instability index	Bond strain index
Magnesiochromite	0.188	0.036
Grossular	0.190	0.066
Diopside	0.108	0.095
Forsterite	0.076	0.042
Fluoro-phlogopite	0.087	0.028
Phlogopite (no H...O)	0.039	0.038
Phlogopite (H...O1,O1,O2)	0.039	0.123
Fluoro-tremolite	0.081	0.042
Tremolite (no H...O)	0.074	0.038
Tremolite (H...O7)	0.073	0.078
Tremolite (H...O7,O6,O6)	0.073	0.091
Albite [7]	0.101	0.048
Albite [8]	0.102	0.047
Albite [9]	0.101	0.047
Epidote (no H...O)	0.126	0.079
Epidote (H...O4)	0.116	0.095

4.2. Structures in which the *a priori* bond valences obey the equal-valence rule exactly

The *a priori* bond valences for magnesiochromite, grossular and forsterite are equal to the Pauling bond strengths (Tables 1, 2 and 4) and there are no bond valence requirements driving any distortion of the bond lengths *via* the effect of the distortion theorem (Brown, 2016; Urusov, 2014; Bosi, 2014; Gagné & Hawthorne, 2017a). Nevertheless, there are significant differences between the *a priori* bond lengths and those observed experimentally. In particular, the observed mean bond lengths are greater than the mean *a priori* bond lengths for all olivine-group minerals, for magnesiochromite and for the Al and Si polyhedra in grossular. There is a significant effect of structure type on the agreement between *a priori* and observed bond lengths and mean bond lengths. This effect was discussed by Bosi (2014) for a handful of minerals and by Gagné & Hawthorne (2017a) for a large number of minerals and synthetic compounds. In particular, Gagné & Hawthorne (2017a) showed close agreement ($R^2 > 0.99$) between the *a priori* and observed mean bond lengths for 14 milarite-group minerals, and found negligible agreement for single ion configurations in many different structure types. For the minerals examined here, we see that within a particular structure type, the agreement between the *a priori* and observed mean bond lengths show systematic deviation from the *a priori* mean bond lengths.

Fig. 2(a) compares the *a priori* and observed $\langle X-O \rangle$ and $\langle Y-O \rangle$ distances for the garnet structures pyrope, almandine, spessartine, calderite, andradite, eringaite, grossular and uvarovite. Both the $\langle X-O \rangle$ ($X = M^{2+}$) and $\langle Y-O \rangle$ ($Y = M^{3+}$) distances are greater than the *a priori* distances for cations of higher

Lewis acidity (Al^{3+} , Mg^{2+}) and less than the *a priori* distances for cations of lower Lewis acidity (Sc^{3+} , Ca^{2+}). Fig. 2(b) compares the *a priori* and observed $\langle M1-O \rangle$ and $\langle M2-O \rangle$ distances for the olivine structures forsterite, fayalite, glaucocroite, liebenbergite, monticellite, tephroite and synthetic $\gamma\text{-Ca}_2\text{SiO}_4$. Both the $\langle M1-O \rangle$ and $\langle M2-O \rangle$ distances are greater than the *a priori* distances; the $\langle M2-O \rangle$ distances scatter about a line that is parallel to the 1:1 line, but the $\langle M1-O \rangle$ distances converge toward the *a priori* distances for cations of lower Lewis acidity (Ca^{2+}).

Here we see an important feature of the relation between *a priori* and observed bond lengths. In the milarite-group minerals, the bond-length correlations differ in detail for the different sites, particularly the *B* site (Gagné & Hawthorne, 2016a). We see the same behaviour here. In the olivine-group silicate minerals, there are separate linear correlations between the *a priori* and observed $\langle M1-O \rangle$ and $\langle M2-O \rangle$ distances. The situation is even more exaggerated in grossular, where there are separate linear correlations for $\langle X-O \rangle$ and $\langle Y-O \rangle$ and the slopes of those correlations deviate significantly from 1.0. In the absence of any driving force for violating the equal-valence rule from *a priori* bond-valence requirements, deviations from the equal-valence rule must come completely from the constraints of embedding the graph representing the ions and bonds into three-dimensional Euclidean space within the constraints of the space-group symmetry adopted by the crystal (Brown, 2016). This indicates that further investigation of the way in which this embedding affects the metric aspects of crystal structures should at first focus on structures in which the *a priori* bond valences obey the equal-valence rule exactly. We suggest that distance-least-squares (Meier & Villiger, 1969) may be a profitable way to approach this problem.

4.3. The effect of hydrogen bonds

The calculations for tremolite with various scenarios for hydrogen bonds can give us an insight into the effect of hydrogen bonds on the calculation of *a priori* bond valences. The calculations were done (1) ignoring hydrogen bonds, (2) with one hydrogen bond to O7, and (3) with one hydrogen bond to O7 and two hydrogen bonds to O6. Agreement between the *a priori* and observed bond lengths is closest when the hydrogen bond(s) is ignored (70%), and the agreement for the remaining bonds is $\sim 10\%$ for one and three hydrogen bonds, with complete disagreement for the hydrogen bonds themselves no matter what the model used. In particular, where hydrogen bonds are taken into account, the *a priori* bond lengths for $\text{H} \cdots \text{O7}$ and $\text{H} \cdots \text{O3}$ ($\times 2$) are 1.760 and 1.769 Å, whereas the corresponding observed values are 2.762 and 2.784 Å. Thus it is apparent that including hydrogen bonds in the *a priori* bond-valence calculation leads to larger disagreement between the *a priori* and observed bond lengths for tremolite. The calculations for epidote are somewhat different. Agreement between the *a priori* and observed bond lengths is approximately the same when the hydrogen bond is ignored and when it is included. Also, there is complete

disagreement for the hydrogen bonds themselves no matter what the model used: the *a priori* $\text{H}^+ \cdots \text{O}^{2-}$ bond lengths are 2.551 Å where the hydrogen bond is omitted and 1.284 Å where the hydrogen bond is included in the calculation, whereas the observed $\text{H}^+ \cdots \text{O}^{2-}$ bond length is 1.973 Å.

Brown (1992, 2016) noted that the equal-valence rule is poorly obeyed in structures containing ions with electronic anisotropies, as the latter can lead to large differences in individual bond lengths within coordination polyhedra. This is the case for H^+ where for [2]-coordination, the bond valences are generally very asymmetric with maxima at 0.859 v.u. (0.983 Å) and 0.138 v.u. (1.764 Å) (Gagné & Hawthorne, 2018). We can see this effect in the relative agreement for the calculations for tremolite and epidote. In tremolite, the $\text{H}^+ \cdots \text{O}^{2-}$ bond is longer at 2.762 Å and in epidote the $\text{H} \cdots \text{O}$ bond is shorter at 1.973 Å, and the infrared spectra in the principal OH-stretching region indicate major differences in the strength of the hydrogen bonding: tremolite (3674 cm^{-1}) (Hawthorne *et al.*, 1996) and epidote ($3100\text{--}3150 \text{ cm}^{-1}$) (Liebscher, 2004). Thus the H environment in tremolite deviates much more from the equal-valence rule than does the H environment in epidote, and the results for tremolite show a greater difference between the *a priori* and observed bond lengths than does epidote for the calculations incorporating the $\text{H}^+ \cdots \text{O}^{2-}$ bond. Thus $\text{H}^+ - \text{O}^{2-}$ bonds generally do not follow the equal-valence rule (Brown, 2016) (which would require two bonds of 0.5 v.u.), and should not be included in the bond network when calculating *a priori* bond valences and bond lengths.

4.4. The effect of uncertain cation coordination numbers

In structures containing alkali metals and alkaline-earth metals with larger coordination numbers, it can be unclear as to what is the most appropriate coordination number. To look at the effect of using different cation coordination numbers on the calculation of *a priori* bond valences, we used albite with Na^+ in coordination numbers of [7], [8] and [9] (Table 14). By-and-large, the effect on the $[\text{AlSi}_3\text{O}_8]$ framework was quite small: the agreement between the *a priori* and observed bond lengths for the framework cations is approximately the same for the different coordination numbers of Na^+ , and the average difference between them is ~ 0.01 Å. On the other hand, the mean range in calculated values for the $\text{Na}^+ - \text{O}^{2-}$ bonds is 0.07 Å and the maximum range is 0.17 Å, and the maximum difference between the *a priori* and observed bond lengths is ~ 0.60 Å. It is apparent that the $\text{Na}-\text{O}$ distances are more susceptible to strain than the higher-valence bonds involving $[\text{AlSi}_3\text{O}_8]$ framework cations, which are of higher Lewis acidity. In general, this suggests that *a priori* and experimental bond lengths will be closer for cations of high Lewis acidity than for cations of low Lewis acidity [see Gagné & Hawthorne (2017b) for values of Lewis acidity].

4.5. Overall comparison of *a priori* and observed bond valences and bond lengths

A comparison of the *a priori* and observed bond valences is shown in Fig. 3(a). The data scatter closely about the 1:1 line with an average deviation of 0.04 v.u. and a maximum deviation of 0.16 v.u. (for the Fe—O8 bond in epidote). Fig. 3(b) shows a comparison of the *a priori* and observed bond lengths. Again the data scatter about the 1:1 line, with an average deviation of 0.048 Å and a maximum deviation of 0.620 Å (for the Na—O5 bond in albite). The scatter of the corresponding *a priori* and observed bond lengths is strongly a function of the Lewis acidity of the constituent cation. Fig. 4 shows that for cations of high Lewis acidity, the range of differences between the *a priori* and observed bond lengths is small, whereas for cations of low Lewis acidity, the range of differences between the *a priori* and observed bond lengths is large.

4.6. Strain in crystal structures

A priori bond valences are calculated by applying the valence-sum rule and the path rule to a bond network with specific formal charges at specific vertices. We may calculate *a priori* bond lengths from the *a priori* bond valences and embed the resulting bond network into three-dimensional Euclidean

space. However, the metric aspects of the bond network are not necessarily maintained in this process, particularly as the structure not only has to fit into three-dimensional Euclidean space but it also has to conform to the symmetry constraints of its space group. The degree-of-fit between an *a priori* structure and the corresponding observed structure is designated as strain, and various definitions have been proposed for this. In particular, the Global Instability Index (GII; Salinas-Sanchez *et al.*, 1992), and the Bond Strain Index (BSI; Preiser *et al.*, 1999) are used to denote this strain. GII is the root-mean-square deviation of the bond-valence sums from their atomic valences, averaged over all atoms in the formula unit

$$\text{GII} = \left(\left(\sum_j s_{ij} - V_i \right)^2 \right)^{1/2},$$

where s_{ij} is the observed bond valence of ion i with coordination number j and V is the formal valence of ion i .

BSI is the root-mean-square deviation between the *a priori* and observed bond valences, averaged over all bonds in the formula unit

$$\text{BSI} = \left(\left(S_{ij} - s_{ij} \right)^2 \right)^{1/2},$$

where S_{ij} is the *a priori* bond valence.

A requirement of calculating BSI is that the *a priori* bond valences must be calculated, and hence BSI has not seen a lot of use as a measure of structural strain. Nevertheless, BSI is a better measure of strain than GII, as GII does not consider the path equations in the calculation of strain. Table 17 gives GII and BSI for the structures examined here. There is a complete lack of correlation ($R^2 = 0.00$) between GII and BSI for all above bonding scenarios combined, and very weak correlation ($R^2 = 0.201$) when omitting structures with hydrogen bonds and the higher coordinations of Na in albite. On the other hand, Gagné & Hawthorne (2016a) showed good correlation ($R^2 = 0.65$) between GII and BSI for 14 milarite-group minerals.

Bosi (2014) and Gagné & Hawthorne (2017a) have suggested that the principal reason for the variation in mean bond length in structures for a specific ion-pair is the result of strain in those structures. It is apparent that the response of different bond topologies to the competing constraints of (1) trying to attain exact accord with the valence-sum rule and the path rule of bond-valence theory, and (2) being constrained to the exact symmetry requirements of various space groups may be very different. If the effect of bond topology on interatomic distances is to be understood, these differences need to be quantitatively understood.

5. Summary

(1) The loop rule of bond-valence theory states that the sum of the directed bond valences around any circuit (closed path) of bonds in a structure is zero. We have found that the sum of the directed bond valences along any path of bonds in a structure is zero where the path begins and ends on symmetrically equivalent terminal ions. Thus we suggest renaming the *loop rule* to the *path rule*: sum of the directed bond valences along

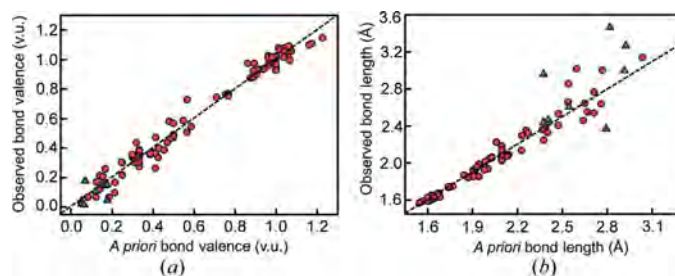


Figure 3 Comparison of (a) *a priori* bond valences with observed bond valences, and (b) *a priori* bond lengths with observed bond lengths for the structures examined here. Blue triangles are for the Na—O bonds of albite. Broken line is $x = y$.

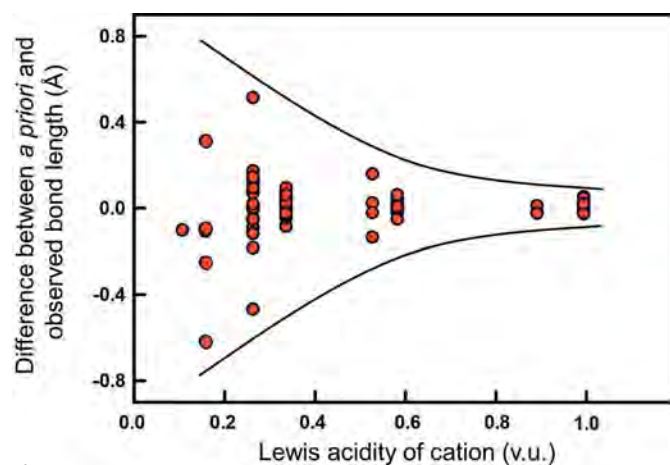


Figure 4 Difference between *a priori* and observed bond lengths as a function of Lewis acidity, showing how the range of differences between *a priori* and observed bond lengths in the structures examined here decreases with increasing Lewis acidity of the constituent cation.

any path of bonds in a structure is zero where the path begins and ends on symmetrically equivalent terminal ions. This more general definition is inclusive of circuits (or loops), as the terminal ions are related by the identity operation.

(2) The valence-sum equations and the path equations of a crystal structure can be solved simultaneously by a simple matrix manipulation to give *a priori* bond valences that can be converted into *a priori* bond lengths using bond-valence curves.

(3) For some low-complexity structures (spinel, garnet), *a priori* bond valences may be calculated from the valence-sum equations alone. For more complex structures (forsterite, diopside, fluoro-phlogopite, tremolite, albite and epidote), the valence-sum equations need to be supplemented by path equations to calculate *a priori* bond valences.

(4) For some structures, there may be some uncertainty as to the coordination number of one or more cations. The effect of using different cation-coordination numbers was examined for low albite with assigned coordination numbers [7], [8] and [9] for Na⁺. Using different coordination numbers for Na⁺ had little effect on the [AlSi₃O₈] framework, and differences between the *a priori* and observed bond lengths are greater than the differences between *a priori* bond lengths calculated for different coordination numbers for Na⁺. A similar effect is seen for structures containing hydrogen bonds.

(5) The *a priori* and observed bond valences and bond lengths scatter closely about $x = y$ with an average deviation of 0.04 v.u. and 0.048 Å and maximum deviations of 0.16 v.u. and 0.620 Å, respectively. The scatter of the corresponding *a priori* and observed bond lengths is strongly a function of the Lewis acidity of the constituent cation. For cations of high Lewis acidity, the range of differences between the *a priori* and observed bond lengths is small, whereas for cations of low Lewis acidity, the range of differences between the *a priori* and observed bond lengths is large.

(6) *A priori* calculation of bond valences and bond lengths allows assessment of the strain in a specific structure and provides a way to examine the effect of bond topology on variation in observed bond lengths for the same ion pair in different bond topologies.

Funding information

The following funding is acknowledged: Natural Sciences and Engineering Research Council of Canada. This work was funded by an NSERC PGS-D3 Scholarship, a UM Duff Roblin and a UM GETS Fellowship to OCG from the University of Manitoba, and a Discovery Grant to FCH from the Natural Sciences and Engineering Research Council of Canada.

References

- Baur, W. H. (1970). *Trans. Am. Crystallogr. Assoc.* **6**, 129–155.
- Baur, W. H. (1971). *Nat. Phys. Sci.* **233**, 135–137.
- Baur, W. H. (1981). In *Structure and Bonding in Crystals*, Vol. 2, edited by M. O'Keeffe and A. Navrotsky, pp 31–52. New York: Academic Press.
- Bosi, F. (2014). *Acta Cryst.* **B70**, 697–704.
- Bosi, F. & Lucchesi, S. (2007). *Am. Mineral.* **92**, 1054–1063.
- Brese, N. E. & O'Keeffe, M. (1991). *Acta Cryst.* **B47**, 192–197.
- Brown, I. D. (1977). *Acta Cryst.* **B33**, 1305–1310.
- Brown, I. D. (1992). *Acta Cryst.* **B48**, 553–572.
- Brown, I. D. (2002). *The Chemical Bond in Inorganic Chemistry*. Oxford University Press.
- Brown, I. D. (2016). *The Chemical Bond in Inorganic Chemistry*, 2nd ed. Oxford University Press.
- Brown, I. D. & Altermatt, D. (1985). *Acta Cryst.* **B41**, 244–247.
- Brown, I. D. & Shannon, R. D. (1973). *Acta Cryst.* **A29**, 266–282.
- Clark, J. R., Appleman, D. E. & Papike, J. J. (1969). *Mineral. Soc. Am. Spec. Pap.* **2**, 31–50.
- Gagné, O. C. & Hawthorne, F. C. (2015). *Acta Cryst.* **B71**, 562–578.
- Gagné, O. C. & Hawthorne, F. C. (2016a). *Can. Mineral.* **54**, 1229–1247.
- Gagné, O. C. & Hawthorne, F. C. (2016b). *Acta Cryst.* **B72**, 602–625.
- Gagné, O. C. & Hawthorne, F. C. (2017a). *Acta Cryst.* **B73**, 1019–1031.
- Gagné, O. C. & Hawthorne, F. C. (2017b). *Acta Cryst.* **B73**, 956–961.
- Gagné, O. C. & Hawthorne, F. C. (2018). *Acta Cryst.* **B74**, 79–96.
- Gatta, G. D., Meven, M. & Bromiley, G. (2010). *Phys. Chem. Miner.* **37**, 475–485.
- Gianfagna, A., Scordari, F., Mazziotti-Tagliani, S., Ventrucci, G. & Ottolini, L. (2007). *Am. Mineral.* **92**, 1601–1609.
- Harlow, G. E. & Brown, G. E. B. Jr (1980). *Am. Mineral.* **65**, 986–995.
- Hawthorne, F. C., Della Ventura, G. & Robert, J.-L. (1996). *Am. Mineral.* **81**, 782–784.
- Hawthorne, F. C. & Grundy, H. D. (1976). *Can. Mineral.* **14**, 334–345.
- Hawthorne, F. C. & Sokolova, E. (2008). *Can. Mineral.* **46**, 1555–1575.
- Krivovichev, S. (2012). *Acta Cryst.* **A68**, 393–398.
- Krivovichev, S. (2013). *Mineral. Mag.* **77**, 275–326.
- Liebscher, A. (2004). *Rev. Mineral. Geochem.* **56**, 125–170.
- Mackay, A. L. & Finney, J. L. (1973). *J. Appl. Cryst.* **6**, 284–289.
- Meagher, E. P. (1975). *Am. Mineral.* **60**, 218–228.
- Meier, W. M. & Villiger, H. (1969). *Z. Kristallogr.* **129**, 411–423.
- Nestola, F., Periotto, B., Andreozzi, G. V., Bruschini, E. & Bosi, F. (2014). *Am. Mineral.* **99**, 1248–1253.
- O'Keeffe, M. (1990). *Acta Cryst.* **A46**, 138–142.
- Papike, J. J., Ross, M. & Clark, J. R. (1969). *Mineral. Soc. Am. Spec. Pap.* **2**, 117–136.
- Preiser, C., Lösel, J., Brown, I. D., Kunz, M. & Skowron, A. (1999). *Acta Cryst.* **B55**, 698–711.
- Rao, G. H. & Brown, I. D. (1998). *Acta Cryst.* **B54**, 221–230.
- Rutherford, J. S. (1990). *Acta Cryst.* **B46**, 289–292.
- Rutherford, J. S. (1998). *Acta Cryst.* **B54**, 204–210.
- Salinas-Sanchez, A., Garcia-Muñoz, J. L., Rodriguez-Carvajal, J., Saez-Puche, R. & Martinez, J. L. (1992). *J. Solid State Chem.* **100**, 201–211.
- Shannon, R. D. (1976). *Acta Cryst.* **A32**, 751–767.
- Smyth, J. R. & Hazen, R. M. (1973). *Am. Mineral.* **58**, 588–593.
- Urusov, V. S. (2014). *J. Struct. Chem.* **55**, 1277–1292.
- Urusov, V. S. & Orlov, I. P. (1999). *Crystallogr. Rep.* **44**, 686–709.